EPJ Web of Conferences **72**, 00010 (2014)
DOI: 10.1051/epjconf/20147200010

Hadron production in e^+e^- collisions at *BABAR* and implications on the muon anomalous magnetic moment

Andreas Hafner[1,a]

[1] *for the BABAR collaboration.*
Institute of Nuclear Physics
J.G.-University Mainz, 55128 Mainz, GERMANY

Abstract. The *BABAR* Collaboration has an intensive program of studying hadronic cross sections at low-energy e^+e^- collisions, accessible via initial-state radiation. Our measurements allow significant improvements in the precision of the predicted value of the muon anomalous magnetic moment. These improvements are necessary for shedding light on the current $\sim 3.5\sigma$ difference between the predicted and the experimental values. We have published results on a number of processes with two to six hadrons in the final state. We report here the results of recent studies with the final states which constitute the main contribution to the hadronic cross section in the energy region between 1 and 3 GeV, as $e^+e^- \to K^+K^-$, $e^+e^- \to K^0_S K^0_L$ and $e^+e^- \to 4$ hadrons.

1 Introduction

The particular interest in hadronic cross section measurements arises due to the discrepancy between the value of the anomalous magnetic moment of the muon $a_\mu = \frac{1}{2}(g-2)_\mu$ obtained by the E821 experiment at BNL [1] and the prediction from the Standard Model [2]. The QED and weak contributions to a_μ can be calculated with very high precision. At low energies perturbation theory cannot be used to calculate the hadronic contribution $a_\mu^{\rm had}$. However, it is possible to relate the hadronic contribution to the muon anomaly $a_\mu^{\rm had}$ via a dispersion relation (Eq. (1)) to hadronic cross sections, which typically are measured in e^+e^- energy scan experiments at low energies.

$$a_\mu^{had,LO} = \frac{1}{4\pi^3}\int_{m_{\pi^o}^2}^{\infty} ds\; K(s)\; \sigma_{e^+e^-\to hadrons}(s). \qquad (1)$$

The Kernel function $K(s)$ is analytically known and proportional to s^{-1} [3].

The study of the Initial State Radiation (ISR) events at B-factories allows independent measurements of these exclusive hadronic cross sections. This method allows high statistics e^+e^- experiments running at a fixed center-of-mass (c.m.) energy to access processes at lower effective c.m. energies by studying events with a high energy photon emitted from the initial state. The use of this technique at high luminosity ϕ- and B-factories has been discussed in detail in Refs. [4–6]. The *BABAR* Collaboration has an extensive program to investigate low multiplicity ISR processes [7] at effective c.m. energies below 5 GeV. In addition to the cross section measurements, these studies include many additional physics topics, e.g. spectroscopy and form-factor measurements.

The ISR cross section for a particular final state f depends on the non-radiative cross section $\sigma_f(s)$, and is obtained from Eq. (2):

$$\frac{d\sigma_{f,\gamma}(m)}{dm} = \frac{2m}{s}\cdot W(s,x,\theta^*_\gamma)\cdot\sigma_f(m), \qquad (2)$$

where $x = \frac{2\cdot E^*_\gamma}{\sqrt{s}}$ and $\sqrt{s}$ is the nominal c.m. energy; θ^*_γ, E^*_γ, and W are the polar angle, energy, and the radiation probability of the ISR photon in the nominal c.m. frame, whereby the effective c.m. energy is decreased to $\sqrt{s'} = m$.

Figure 1 shows the relative distribution of contributions (left) and uncertainties (right) for $a_\mu^{\rm had}$ from different energy regions [8]. The low energy contributions are of high importance, e.g. the process $e^+e^- \to \pi^+\pi^-$ contributes with approximately 73% to $a_\mu^{\rm had}$. Due to the very precise measurement of the leading contribution to $a_\mu^{\rm had}$, the leading contribution to the uncertainty stems from the region between 1 GeV and 2 GeV.

The four-pion and two-kaon channels are the most significant in this region of interest. The results of the $\pi^+\pi^-\pi^+\pi^-$, K^+K^-, and $K^0_S K^0_L$ analyses are presented here. The measurement of $e^+e^- \to \pi^+\pi^-\pi^0\pi^0$ is still preliminary, but will be finalised and published soon. We also present the first measurement of the channels $e^+e^- \to K^0_S K^0_L \pi^+\pi^-$, $e^+e^- \to K^0_S K^0_S \pi^+\pi^-$, and $e^+e^- \to K^0_S K^0_S K^+K^-$.

2 The *BABAR* experiment

The Stanford Linear Accelerator (SLAC) provided 9 GeV electrons and 3.1 GeV positrons to the asymmetric-energy

[a] e-mail: hafner@kph.uni-mainz.de

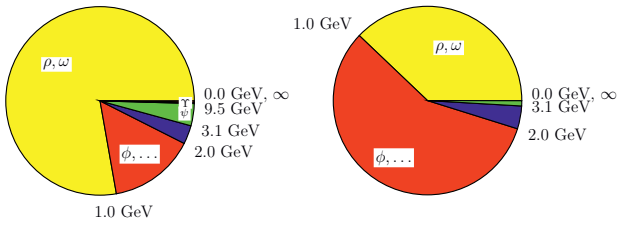

Figure 1. The distribution of contributions (left) and uncertainties (right) in % for $a_\mu^{\rm had}$ from different energy regions [8]. The error is $\sigma^2_{itot}/\Sigma_i\sigma^2_{itot}$ in %. The total error combines statistical and systematic errors in quadrature.

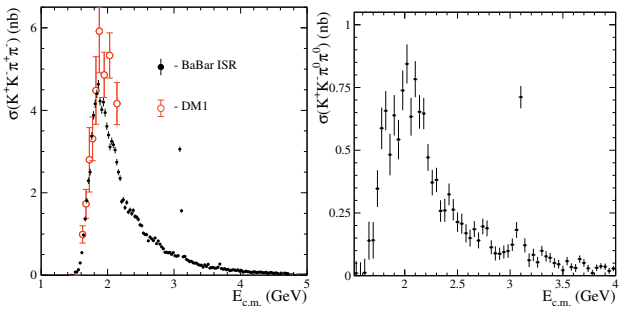

Figure 2. Cross section for the process $e^+e^- \to K^+K^-\pi^+\pi^-$ (left) and $e^+e^- \to K^+K^-\pi^0\pi^0$ (right) for the entire energy range. Only statistical errors are indicated.

PEP-II e^+e^- collider. This corresponds to a c.m. energy of $\sqrt{s} = 10.58$ GeV, the mass of the $\Upsilon(4S)$ resonance. Approximately 10% of the data were recorded at c.m. energy of 10.54 GeV to enable background studies. The *BABAR* detector is described elsewhere [9]. The reconstruction of charged-particle tracks is performed in the tracking system, which comprises a five-layer silicon vertex tracker (SVT) and a 40-layer drift chamber (DCH) in a 1.5 T axial magnetic field. Separation of charged pions, kaons, and protons is achieved with a combination of Cherenkov-angle measurements in the detector of internally reflected Cherenkov light (DIRC) and specific ionization measurements in the SVT and DCH. The CsI(Tl) electromagnetic calorimeter (EMC) measures the energy of photons and electrons. Muon identification is provided by the instrumented flux return (IFR) in order to select $\mu^+\mu^-\gamma$ final state events, which are used in order to normalize the $\pi\pi$ cross section.

A simulation package developed for radiative processes, AfkQed, is used to study the detector acceptance and efficiency. The simulation of hadronic final states is based on an approach suggested by Czyż and Kühn [10]. Additional ISR photons are generated with the structure function method [11], and additional FSR photons with PHOTOS [12]. The ISR background channels simulated with AfkQed have been studied, as have non-radiative continuum background events from $e^+e^- \to q\bar{q}$ (q = u,d,s,c), generated with JETSET [13]. The response of the *BABAR* detector is simulated with Geant4 [14]. The generated events are subjected to detector simulation, and are reconstructed with the same software chain used for experimental data events. Variations in detector and background conditions over the course of the experiment are taken into account. The detection efficiency obtained by simulation is then corrected by extensive studies of differences between data and MC. Separate studies have been performed in order to determine the tracking and particle identification efficiencies.

2.1 $e^+e^- \to \pi^+\pi^-$ cross section

The obtained detection efficiency (acceptance) by simulation is then corrected by extensive studies of differences between data and MC. Separate studies have been performed in order to detemine the tracking and PID efficiencies. Specifically for the $e^+e^- \to \pi^+\pi^-$ final state, the systematic uncertainties listed in Table 1 are all determined with an accuracy of a few permil.

Source of Uncertainty	CM Energy Interval (GeV)				
	0.3-0.4	0.4-0.5	0.5-0.6	0.6-0.9	0.9-1.2
trigger/ filter	5.3	2.7	1.9	1.0	0.5
tracking	3.8	2.1	2.1	1.1	1.7
π-ID	10.1	2.5	6.2	2.4	4.2
background	3.5	4.3	5.2	1.0	3.0
acceptance	1.6	1.6	1.0	1.0	1.6
kinematic fit (χ^2)	0.9	0.9	0.3	0.3	0.9
correlated $\mu\mu$ ID loss	3.0	2.0	3.0	1.3	2.0
$\pi\pi/\mu\mu$ non-cancel.	2.7	1.4	1.6	1.1	1.3
unfolding	1.0	2.7	2.7	1.0	1.3
ISR luminosity ($\mu\mu$)	3.4	3.4	3.4	3.4	3.4
total uncertainty	13.8	8.1	10.2	5.0	6.5

Table 1. Relative systematic uncertainties (in 10^{-3}) on the $e^+e^- \to \pi^+\pi^-(\gamma)$ cross section by $\sqrt{s'}$ intervals (in GeV) up to 1.2 GeV. The statistical part of the efficiency uncertainties is included in the total statistical uncertainty in each interval.

In standard *BABAR* ISR analyses, the high energetic photons $E_{\gamma,ISR}$ are detected at large angles. In the $\pi^+\pi^-$ study the charged π-pair can be accompanied by a final state radiation (FSR) photon, which is included in the analysis. The data used in the $\pi^+\pi^-$ analysis amounts to a total integrated luminosity of 232 fb^{-1}. The $\pi^+\pi^-$ cross section is obtained from the ratio of pion to muon yield. This decreases systematic uncertainties, since effects due to the photon efficiency, the luminosity measurement, the theoretical radiator function or the vacuum polarisation cancel in the ratio. As a cross-check the measured muon cross section is compared to the QED prediction. The result of this QED test can be seen in equation 3 or as a function of the effective c.m. energy in Fig. 3.

$$\frac{\sigma^{data}_{\mu\mu\gamma(\gamma)}}{\sigma^{data}_{\mu\mu\gamma(\gamma)}} - 1 = (40 \pm 20 \pm 55 \pm 94) \cdot 10^{-4} \qquad (3)$$

The resulting $\pi^+\pi^-$ cross section with the dominant ρ peak can be observed in Fig. 3(b). The zoom in Fig. 3(c) shows an edge on the right hand side of the peak, which is due to the $\rho - \omega$ interference. The systematic uncertainty in this region is 0.5%. Between 1.5 and 1.6 GeV a dip due to interference with a higher ρ resonance is seen as well as another dipping structure at around 2.2 GeV.

The $\pi\pi$ cross section measured by various experiments is displayed in Fig. 4 (top). The KLOE experiment also has a systematic uncertainty bellow 1%. Fig. 4 (bottom) compares the *BABAR* and KLOE experiments to the

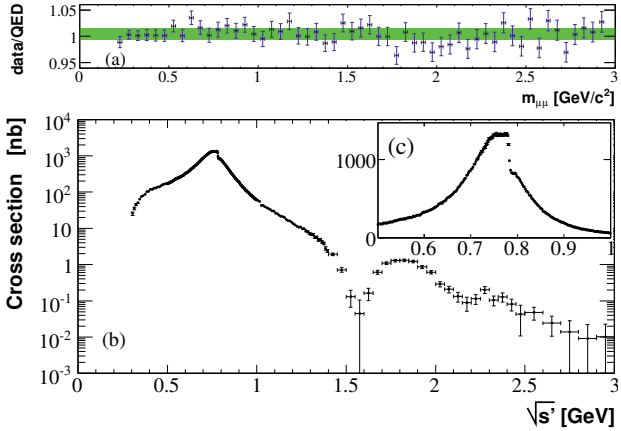

Figure 3. (a) The ratio of the measured cross section for $e^+e^- \to \mu^+\mu^-\gamma(\gamma)$ to the NLO QED prediction. Eq. 3 is represented by the green band. (b) The measured cross section for $e^+e^- \to \pi^+\pi^-(\gamma)$ from 0.3 to 3 GeV. (c) Enlarged view of the ρ region in energy intervals of 2 MeV. The plotted errors are from the sum of the diagonal elements of the statistical and systematic covariance matrices.

HVPTools [15] average. These two experiments dominate this average and in the energy interval between 0.63 and 0.958 GeV, the discrepancy between the $a_\mu^{had,LO}[\pi\pi]$ evaluations from KLOE and *BABAR* amounts to 2.0 σ.

As mentioned, and shown in Fig. 1, due the very precise measurements of the leading contribution from the final state $e^+e^- \to \pi^+\pi^-$ to the integral of a_μ^{had}, the leading contribution to the uncertainty δa_μ^{had} comes now from the region between 1 GeV and 2 GeV. Here, the four-pion and two-kaon final states dominate the total contribution to a_μ^{had}.

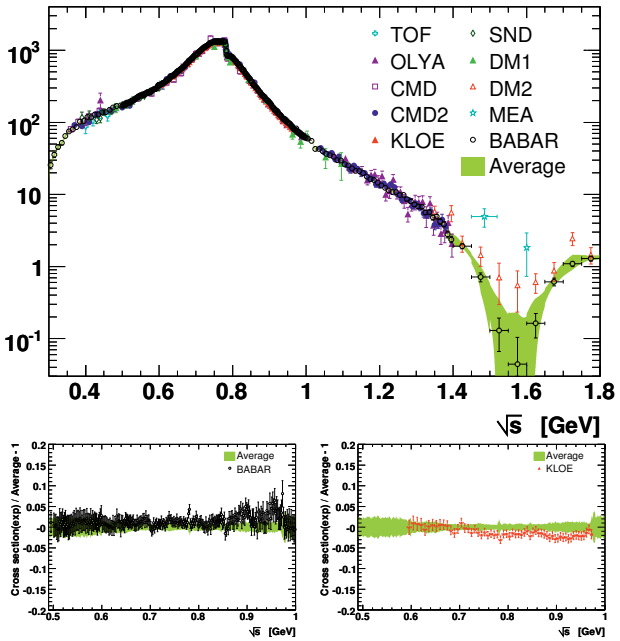

Figure 4. Cross section of the process $e^+e^- \to \pi^+\pi^-$ measured by different experiments for the entire energy range (top). Relative cross section comparison between the HVPTools average (shaded band) and the *BABAR* (left) and KLOE (right) measurements.

2.2 $e^+e^- \to \pi^+\pi^-\pi^+\pi^-$

The data used in the following analyses correspond to a total integrated luminosity of 454 fb^{-1}. In standard *BABAR* ISR analyses, the high energy photons are detected at large angles with respect to the e^+e^- collision axis. Concerning the $\pi^+\pi^-\pi^+\pi^-$ final state, the cross section is shown in Fig. 5. The systematic uncertainty of this measurement is 2.4% in the peak region, increasing to 10.7% in the low energy region shown in the inlay, and to 5.5% (8.5%) for energies above 2.8 GeV (4.0 GeV).

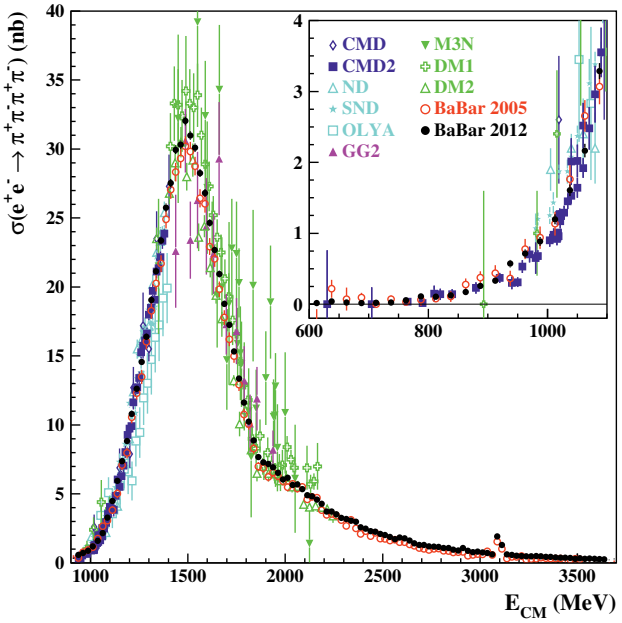

Figure 5. Cross section for the process $e^+e^- \to \pi^+\pi^-\pi^+\pi^-$ measured by different experiments for the entire energy range. Only statistical errors are shown.

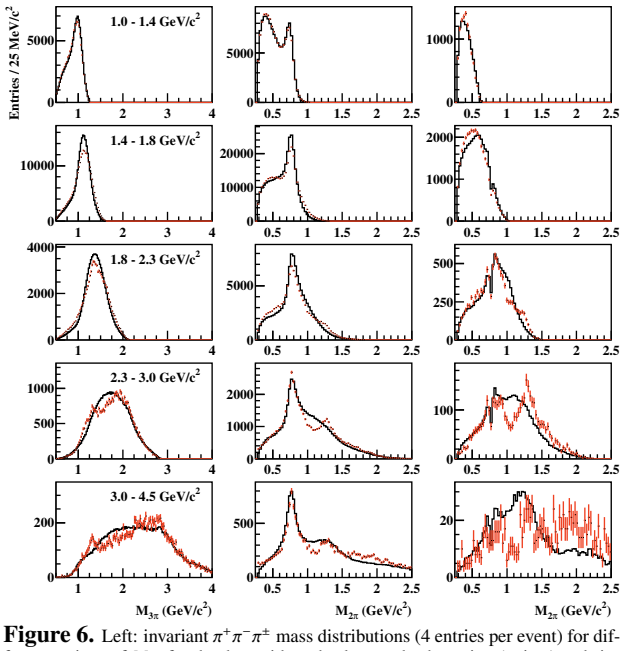

Figure 6. Left: invariant $\pi^+\pi^-\pi^\pm$ mass distributions (4 entries per event) for different regions of $M_{4\pi}$ for the data without background subtraction (points) and signal simulation (histogram); Middle: $\pi^+\pi^-$ mass distributions (4 entries per event); Right: the $\pi^+\pi^-$ mass distribution with the other $\pi^+\pi^-$ mass in the $\rho(770)^0$ mass region.

This final state also contains various intermediate resonances. The $\pi^+\pi^-\pi^\pm$ invariant mass distribution is shown

in the leftmost column of Fig. 6 for different regions of 4π mass. In the low mass region, $1.0 < M_{4\pi} < 1.4\,\mathrm{GeV}/c^2$, there is not enough energy to allow production of the $a_1(1260)^{\pm}$. At higher $M_{4\pi}$, the contribution of the $a_1(1260)^{\pm}$ becomes visible. It is observed as a peaking structure with mass and width $M_{3\pi} \approx 1300\,\mathrm{MeV}/c^2$ and $\Gamma \approx 200\,\mathrm{MeV}$, respectively. In the $\pi^+\pi^-$ invariant mass distributions shown in the middle column of Fig. 6, four entries are present per event. At low 4π mass and in the peak region only a single resonance, the $\rho(770)^0$, is observed. At larger 4π mass, a second peaking structure appears at $M_{2\pi} \approx 1270\,\mathrm{MeV}/c^2$, which most likely corresponds to the $f_2(1270)$. Approximately 25% of the entries are in the $\rho(770)^0$ peak. The production of $\rho(770)^0\rho(770)^0$ via a single virtual photon is not allowed due to C-parity conservation (but see Ref. [16]), leading to the conclusion that in each event one $\rho(770)^0$ meson is present. To investigate the possible presence of the $f_2(1270)\rho(770)^0$ final state, the $\pi^+\pi^-$ combination is plotted for the case that there is another $\pi^+\pi^-$ combination within $\pm 25\,\mathrm{MeV}/c^2$ of the $\rho(770)^0$ mass (Fig. 6, right column). The $f_2(1270)$ resonance is visible as a shoulder in the $1.8 < M_{4\pi} < 2.3\,\mathrm{GeV}/c^2$ mass region. It is even more prominent in the $2.3 < M_{4\pi} < 4.5\,\mathrm{GeV}/c^2$ region, where the energy is large enough to allow direct production of $f_2(1270)\rho(770)^0$. A sharp falloff in the $M_{2\pi}$ spectrum just below $1\,\mathrm{GeV}/c^2$ is visible in the $1.8 < M_{4\pi} < 2.3\,\mathrm{GeV}/c^2$ region. This might be due to interference with the $f_0(980)$ final state. A partial wave analysis would be necessary to determine the amplitude structure of the individual intermediate states.

2.3 $e^+e^- \to K^+K^-$

The cross section of $e^+e^- \to K^+K^-$ is shown in Fig. 7 (top). The $\phi(1020)$ as well as additional structures between 1.7 and 2.3 GeV are clearly visible. In the $\phi(1020)$ peak region, the uncertainty is 0.8%. The J/ψ and $\psi(2S)$ are excluded from this plot. From the cross section the effective form factor is extracted and shown in Fig. 7 (middle) with a fit based on a model with a sum of resonances [17] and with an additional zoom on the ϕ-resonance Fig. 7 (bottom).

From this fit the mass $m_\phi = 1019.51 \pm 0.02 \pm 0.05_{sys}\,\mathrm{MeV}/c^2$ and width $\Gamma_\phi = 4.29 \pm 0.04 \pm 0.06_{sys}\,\mathrm{MeV}$ of the ϕ resonance are extracted. These are in agreement with the PDG values. From the integrated ϕ peak, the partial electronic width:

$$\Gamma_\phi^{ee} \times \mathcal{B}(\phi \to K^+K^-) = \frac{\alpha^2\beta^3(s, m_K)}{324}\frac{m_\phi^2}{\Gamma_\phi}a_\phi^2 C_{FS}$$

$$= 0.6344 \pm 0.0059_{exp} \pm 0.0028_{fit} \pm 0.0015_{cal}\,\mathrm{keV}$$

can be measured.

This fit can also be used to compare the *BABAR* data to the existing measurements. The comparison shows a difference of approximately 1.5-2.5 standard deviations in the absolute normalization to the Novosibirsk measurements of CMD-2 and SND.

At large momentum transfers, our data of the form factor measurement can be compared to QCD predictions in the asymptotic regime. A power law of $F_K \propto \alpha_S(Q^2)Q^{-n}$ with $n = 2$ is predicted by [18]. The data is in perfect agreement with the power law: in the momentum transfer region Q=2.5-5 GeV, we extract $n = 2.10 \pm 0.23$ from the fit. However the absolute normalization is a factor of 20 higher than the predicted curve. There is no trend in data up to $Q^2 = 25\,\mathrm{GeV}^2$ for approaching the asymptotic QCD prediction. The CLEO measurements [19, 20] are in very good agreement with our data.

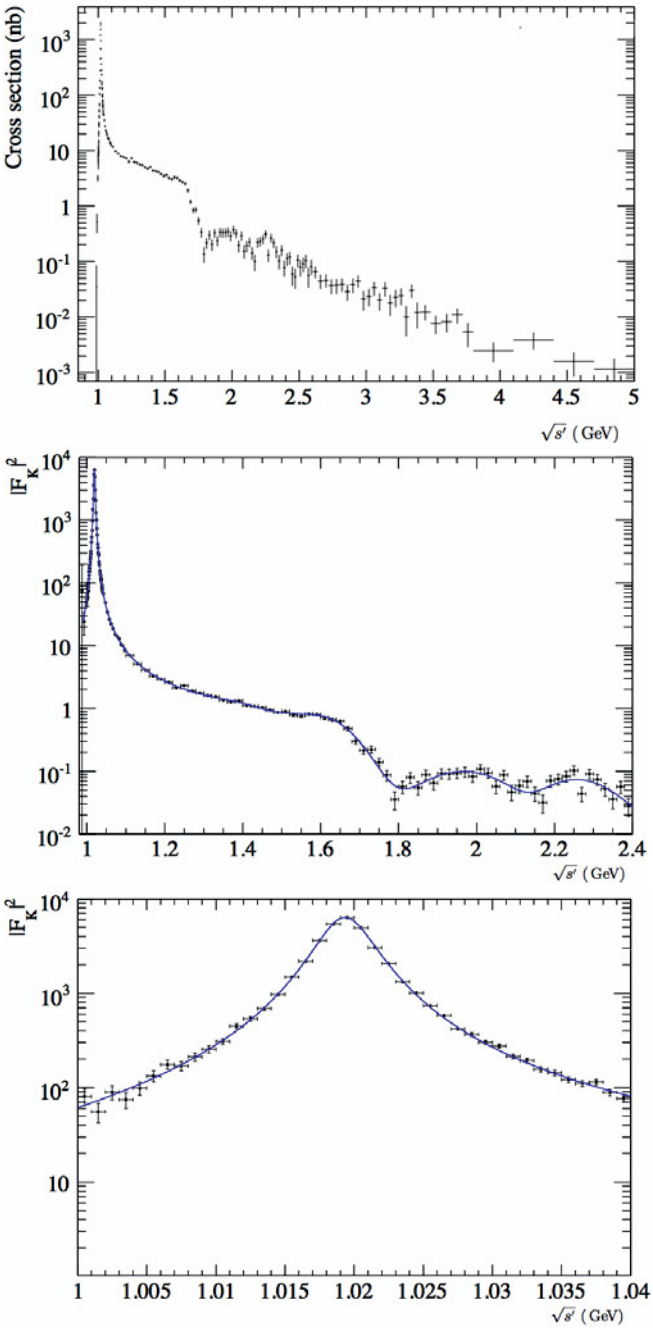

Figure 7. Top: Cross section of $e^+e^- \to K^+K^-$. Middle: Charged kaon form factor with a phenomenological fit. Bottom: Charged kaon form factor with an additional zoom on the $\phi(1020)$ peak.

Table 2. Extracted parameters from the fit to the $K_S^0K_L^0$ invariant mass distribution in the ϕ region. Red parameters are directly extracted from the fit, blue parameters require additional input from the PDG as indicated. Concerning the uncertainties of the red *BABAR* parameters, the first are statistical, the second systematic, and the third due to model dependence, varying the cross sections of the background contributions by their corresponding uncertainties.

	BABAR	CMD-2	PDG(2012)
σ_0[nb]	1409 ± 33 ± 42 ± 15	1376 ± 6 ± 23	-
m_ϕ[MeV/c^2]	1019.46 ±0.04 ± 0.05 ± 0.03	1019.48 ±0.01 ± 0.03	1019.46 ±0.02
Γ_ϕ[MeV]	4.205 ±0.103 ± 0.050 ± 0.045	4.280 ±0.033 ± 0.025	4.26 ±0.04
$\Gamma_\phi^{ee}\mathcal{B}_{K_S^0K_L^0}$[keV]	0.4200 ±0.0033 ± 0.0122 ± 0.0019	-	-
Γ_ϕ^{ee}[keV]	1.228 ±0.037 ± 0.0140$^{PDG}_{\mathcal{B}(\phi\to K_S^0K_L^0)}$	1.235 ± 0.006 ± 0.022	1.27 ± 0.04
$\mathcal{B}_{ee}\mathcal{B}_{K_S^0K_L^0}\cdot 10^4$	0.986 ±0.030 ± 0.009$^{PDG}_{\Gamma_\phi}$	-	1.006 ± 0.016

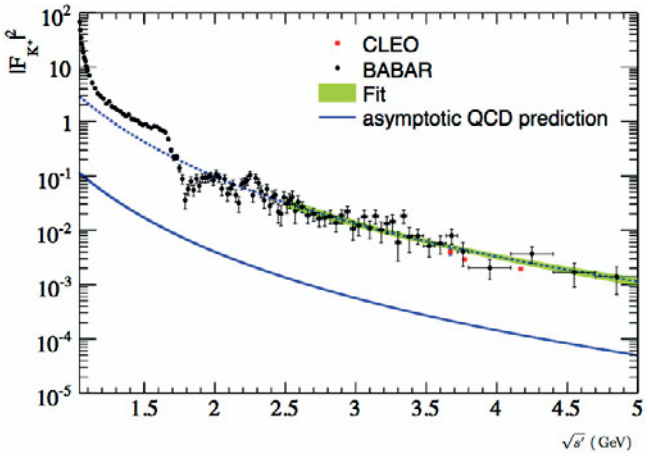

Figure 8. Charged kaon form factor (black points) with a fit to the data (green line), the theoretical prediction for the asymptotic regime (blue line), and the CLEO data (red squares).

2.4 $e^+e^- \to K_S^0K_L^0$, $K_S^0K_L^0\pi^+\pi^-$, $K_S^0K_S^0\pi^+\pi^-$, $K_S^0K_S^0K^+K^-$

Preliminary results on these four final states have been presented. The standard event selection for *BABAR* ISR-analyses has been applied. In addition the $K_S^0 \to \pi^+\pi^-$ are detected via two tracks in the fiducial detector volume with a veto on electrons according to particle identification requirements. A vertex fit for the K_S^0 is applied and the flight length (FL) is restricted to 0.2 cm $< FL <$ 40 cm. The invariant mass of the two pions is restricted to the K_S^0 mass: 0.472 MeV/c^2 $< m(K_S^0) <$ 0.522 MeV/c^2. K_L^0 are detected as signal in the electromagnetic calorimeter. The detection probability of the K_L^0 in the fiducial volume of the detector is approximately 50%. Efficiency differences between the data and simulation have been studied in detail for events from the $\phi \to K_S^0K_L^0$ signal.

The cross section and parameters of the ϕ resonance are extracted from a fit to the invariant mass distribution, which is shown in Fig. 9 (top). The accuracy of the preliminary cross section measurement of $e^+e^- \to K_S^0K_L^0$ is below 3% in this ϕ peak region.

The cross section above the dominant ϕ resonance is shown in Fig. 9 (bottom). The systematic uncertainty is dominated by the background subtraction procedure and reaches approximately 10% (30%) for the regions with $\sigma >$ 0.5 nb ($\sigma <$ 0.5 nb).

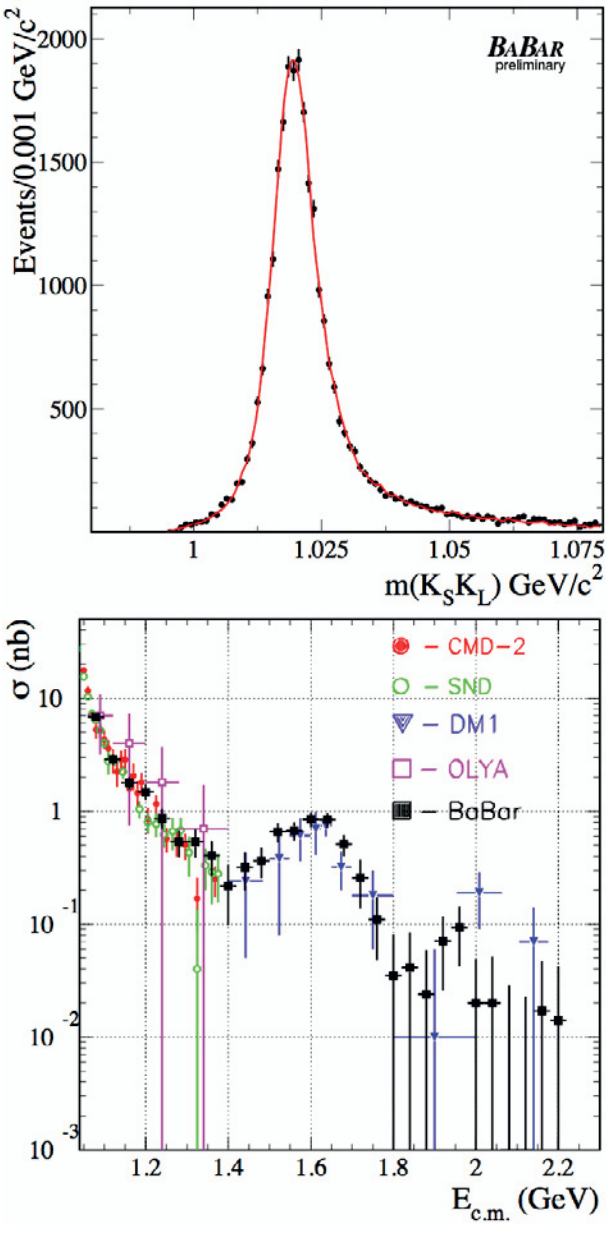

Figure 9. Preliminary results for the measurement of the $K_S^0K_L^0$ invariant mass distribution around the $\phi(1020)$ peak (top) and the $K_S^0K_L^0$ cross section above the $\phi(1020)$ resonance (bottom) in comparison to the existing data.

Cross section measurements of two neutral kaons with additional kaons and pions in the final state have not been measured up to date. The first measurement of the cross section for the final states $e^+e^- \to K^0_S K^0_L \pi^+\pi^-$ (top), $K^0_S K^0_S \pi^+\pi^-$ (middle), and $K^0_S K^0_S K^+K^-$ (bottom) can be seen in Fig. 10. From these measurements, we are also able to extract the corresponding branching ratios of the J/ψ: $\mathcal{B}_{J/\psi \to K^0_S K^0_L \pi^+\pi^-} = (3.7 \pm 0.6 \pm 0.4) \cdot 10^{-3}$, $\mathcal{B}_{J/\psi \to K^0_S K^0_S \pi^+\pi^-} = (1.68 \pm 0.16 \pm 0.08) \cdot 10^{-3}$, and $\mathcal{B}_{J/\psi \to K^0_S K^0_S K^+K^-} = (0.42 \pm 0.08 \pm 0.02) \cdot 10^{-3}$.

2.5 Influence of *BABAR* data on a_μ

Fig. 11 shows an update of the theoretical predictions for a_μ. Without the newest *BABAR* measurements a 3.7 σ difference between the experimental and the theoretical value for a_μ exists. Including the *BABAR* results for the $\pi^+\pi^-$ cross section a deviation of 3.2 σ remains. Using only the *BABAR* data leads to 2.4 σ. There is a basic difference between *BABAR* and KLOE ISR analyses, i.e. KLOE runs on the ϕ resonance at 1.02 GeV, while *BABAR* runs at the $\Upsilon(4S)$ resonance at 10.58 GeV. Therefore the two experiments have different FSR corrections and also different FSR background contributions.These differences are still under investigation.

The contribution to a_μ^{had} from $e^+e^- \to \pi^+\pi^-\pi^+\pi^-$ based solely on the *BABAR* measurement is estimated to be $a_\mu^{had}(\pi^+\pi^-\pi^+\pi^-) = (13.35 \pm 0.10_{stat} \pm 0.52_{syst}) \cdot 10^{-10}$. The corresponding evaluation of the K^+K^- final state leads to $a_\mu^{had}(K^+K^-) = (22.95 \pm 0.14_{stat} \pm 0.22_{syst}) \cdot 10^{-10}$. These measurements reduce the corresponding estimated uncertainty without the *BABAR* data by approximately a factor of 3. The evaluation of the $K^0_S K^0_L$ *BABAR* data and the combination of the K^+K^- and $\pi^+\pi^-\pi^+\pi^-$ final states with other existing measurements still remains do be done.

3 Conclusions

ISR physics, including measurements of hadronic cross sections, is a very productive field in addition to B-physics at *BABAR*. Many measurements were performed for the first time with high accuracy and are important for the theoretical prediction of a_μ. The $\pi^+\pi^-$ channel with a contribution of 73% for the hadronic part of the muon anomaly was measured with a precision below 1% and with 0.5% in the peak region. The measurements of the final states $\pi^+\pi^-$ and K^+K^- reduces the existing uncertainty of these channels by a factor of 3. The evaluation of the contribution of the channel $e^+e^- \to K^0_S K^0_L$ is not yet performed. The remaining difference between the theoretical prediction and the measured value of a_μ of 3-4 σ still poses an open question and needs further studies.

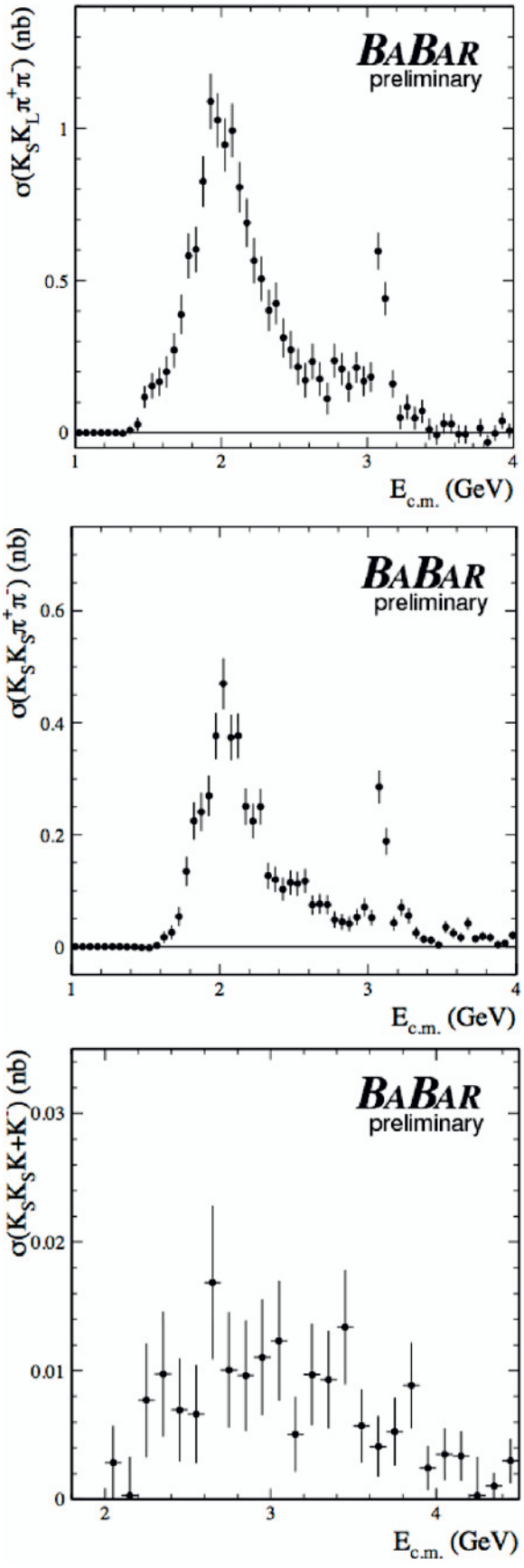

Figure 10. Preliminary results for the measurement of the cross section of the reaction $e^+e^- \to K^0_S K^0_L \pi^+\pi^-$ (top), $K^0_S K^0_S \pi^+\pi^-$ (middle), and $K^0_S K^0_S K^+K^-$ (bottom).

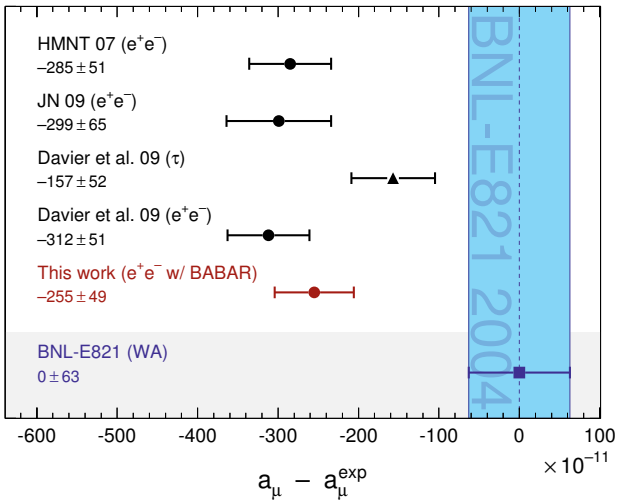

Figure 11. Compilation of recent results for a_μ^{SM}, subtracted by the central value of the experimental average [1]. The shaded vertical band indicates the experimental error. The SM predictions are taken from: HMNT 07 [21], JN 09 [8], Davier *et al.* [15] (τ-based and e^+e^- including KLOE), and the e^+e^--based value from this work.

Acknowledgements

I wish to thank the organising committee of the LHPMF conference for the warm hospitality. I am also grateful to my colleagues from the *BABAR* collaboration for their input to my presentation and these proceedings.

References

[1] G.W. Bennett *et al.* (Muon g-2 Collaboration), Phys. Rev. D **73**, 072003 (2006).

[2] M. Davier (Orsay, LAL), S. Eidelman (Novosibirsk, IYF), A. Hocker, Z. Zhang (Orsay, LAL). LAL-03-50, Aug 2003. 14pp., Eur.Phys.J.C31:503-510,2003 e-Print Archive: hep-ex/0308213.

[3] S.J. Brodsky and E. de Rafael, Phys. Rev. **168**, 1620 (1968).

[4] A.B. Arbuzov *et al.*, JHEP **9812**, 009 (1998).

[5] S. Binner, J.H. Kühn, K. Melnikov, Phys. Lett. B **459**, 279 (1999).

[6] M. Benayoun *et al.*, Mod. Phys. Lett. A **14**, 2605 (1999).

[7] B. Aubert *et al.* (*BABAR* Collaboration), PRD **70**, 072004 (2004) , PRD **71**, 052001 (2005) , PRD **73**, 052003 (2006) , PRD **73**, 012005 (2006) , PRD **76**, 092006 (2007) , PRD **76**, 092005 (2007) , PRD **76**, 012008 (2007) , PRD **77**, 092002 (2008) , PRL **103**, 231801 (2009) , PRD **85**, 112009 (2012) , PRD **86**, 012008 (2012) , PRD **86**, 032013 (2012) , PRD **88**, 032013 (2013).

[8] F. Jegerlehner and A. Nyffeler, Phys.Rept. **477**, 1 (2009).

[9] B. Aubert *et al.* (*BABAR* Collaboration), Nucl.Instr.Meth. PR A **479**,1 (2002).

[10] H. Czyż and J.H. Kühn, Eur.Phys.J C **18**, 497 (2000).

[11] M. Caffo, H. Czyż, E. Remiddi, Nuo. Cim. A **110**, 515 (1997); Phys. Lett. B **327**, 369 (1994).

[12] E. Barberio, B. van Eijk and Z. Was. Comput. Phys. Commun. **66**, 115 (1991).

[13] T. Sjöstrand, Comput. Phys. Commun. **82**, 74 (1994).

[14] S. Agostinelli *et al.* (Geant4 Collab.), Nucl. Instrum. Methods Phys. Res., Sect. A **506**, 250 (2003).

[15] M. Davier *et al.*, Europ. Phys. J. C **71**, 1515 (2011).

[16] B. Aubert et *et al.* (*BABAR* Collaboration), PRL **97**, 112002 (2006).

[17] C. Bruch, A. Khodjamirian, and J.H. Kühn, Eur.Phys.J. **C24**, 41 (2005).

[18] S.J. Brodsky and G.P. Lepage, Phys.Lett. **B87**, 359 (1979).

[19] T.K. Pedlar et al., Phys.Rev.Lett. **95**, 261803, 2005.

[20] K.K. Seth et al. (CLEO Collaboration), arXiv:1210.1596 [hep-ex].

[21] T. Teubner, K. Hagiwara, R. Liao, A.D. Martin, D. Nomura, Nucl.Phys.Proc.Suppl. **218**, 225 (2011).